Cite this paper as : D. Zheng, T. Pauporté, Control by Mixed-Chloride Additives of the Quality and Homogeneity of Bulk Halide Perovskite upon Film Formation Process. J. Mater Chem. A 9 (2021) 17801-17811.

# Control by Mixed-Chloride Additives of the Quality and Homogeneity of Bulk Halide Perovskite upon Film Formation Process

*Daming Zheng and Thierry Pauporté**

Chimie ParisTech, PSL Research University, CNRS, Institut de Recherche de Chimie Paris (IRCP), UMR8247, 11 rue P. et M. Curie, F-75005 Paris, France.

*Corresponding author, email: thierry.pauporte@chimieparistech.psl.eu

Website: www.pauportegroup.com

KEYWORDS: Perovskite solar cells, Film formation control and mechanism, Chloride additives, Glow discharge Optical Emission Spectroscopy, Methylammonium-free perovskite

**ABSTRACT:** Nowadays, overcoming the stability issue of perovskite solar cells (PSCs) while keeping high efficiency has become an urgent need for the future of this technology. By using x-ray diffraction (XRD), scanning electron microscopy (SEM), differential Scanning Calorimetry (DSC) and introducing solvent profile evolution monitoring by glow discharge optical emission spectroscopy (GD-OES) technique, we have highlighted the effect of chloride additives on the formation mechanism of $Cs_{0.1}FA_{0.9}PbI_3$ films upon annealing. Two formation steps are distinguished: first the superficial residual solvent is eliminated, second, the solvent in the depth of the film is evaporated. The elimination profile signs the final morphology of the layer. The downward (top-down) growth has been encountered for the pristine and potassium chloride additive cases. It led to the formation of multiple boundaries and middle-sized grain morphology. We unveil that employing both potassium chloride and ammonium chloride additives forces the homogeneous elimination of the solvent across the layer, and then the lateral growth of the grains. It resulted in large size, monolithic and defect-poor grains with good coverage of the substrate which are the targeted properties for high efficiency. By combining this approach with the film surface treatment with *n*-propylammonium iodide (PAI), further performance and stability increases have been achieved. It resulted in a stabilized power conversion efficiency over 21%. These PSCs are also proved to be highly resistant to light, moisture, and temperature external stressors.

# 1. Introduction

Photovoltaic (PV) solar cells still need improvement for cost-effectiveness, saving of raw material and gain in pay-back energy consumption. Beyond the now mature silicon technologies, solid-state halide perovskite (PVK) solar cells (PSCs) have emerged during the last years as a possible alternative or complementary PV technology.[1-9] Single junction PSCs achieve a present 25.5% record power conversion efficiency (PCE) [10] which is the best among the thin film technologies and closely approaches the best single crystalline silicon ones. However, the wide deployment of PSCs still needs a significant improvement in their stability since classical PVKs are sensitive notably to moisture, oxygen and heat, while efficiency must be kept high. Most of these agents initiate degradation of PVK films at the grain boundaries.

A great strength of PSCs is that the perovskite functional layer is prepared at mild temperature (≤160°C) from perovskite precursor solutions (PPSs). The chemistry of these solutions is key for the final properties of the absorber film and PPSs must be formulated with care to optimize the final PV properties of the films. They contain two kinds of important components for the final PSC performance, (i) those which will form the film and will define the final composition of the layer; (ii) those that help the synthesis of the film and are eliminated upon the final annealing step. They are dissolved in polar aprotic organic solvents. By working on this chemistry and on the crystallization control, the device performance, as well as the material thin film stability, can be dramatically increased, not only by reaching the intrinsic entropic stabilization, but also by enhancing the crystallinity, suppressing defect formation, and stabilizing grain boundaries. Additives have a key role in the film formation which remain to be deeply understood. Especially, synergistic effect, that can arise when two additives are combined in the PPS, is intriguing and promising for the future of the PSC technology. They allow to reach the target films properties which are full-coverage, pinhole-freeness, well-crystallization of films composed of large grains. These characteristics are reached by finely controlling the nucleation and growth of the perovskite grains forming the film during the annealing treatment.[11,12] At this stage, the amount of grain boundaries as well as the structural and grain boundaries defects such as Frenkel ones[13] must be drastically limited.[14-16]

The present paper focuses on the simple $Cs_{0.1}FA_{0.9}PbI_3$ perovskite. From the point of view of the composition, methylammonium ($MA^+$)-free PVKs are desirable since $MA^+$ can decompose with heating, outgases with time and is hygroscopic while this composition must also avoid halide mixture which can be at the origin of phase separation.[17-28] We show that the use of ammonium chloride and potassium chloride mixed PPS additives control the crystallization and leads to the desirable lateral growth of the perovskite films. Their mixture allows the formation of an initial yellow translucent layer after a one-step spin-coating with dripping chlorobenzene antisolvent. This layer contains $Cs_{0.1}FA_{0.9}PbI_3$ in a δ-phase and, also, in the α-phase in a significant amount combined with wetting solvent. By using x-ray

diffraction (XRD), scanning electron microscopy (SEM), differential scanning calorimetry (DSC) and introducing solvent profile evolution monitoring by glow discharge-optical emission spectroscopy (GD-OES) technique, we unveil the formation mechanism of the films upon annealing. Two formation phases are distinguished: first the superficial residual solvent is eliminated, prior to the solvent in the depth of the film. The elimination profile signs the final morphology of the layer. We show that when the chloride mixture is employed, the solvent is homogeneously eliminated across the layer, leading to a lateral growth of the grains. It results in large, monolithic and defect-poor grains with good coverage of the substrate. By combining this approach with the film surface treatment with n-propylammonium iodide (PAI), further performance and stability increase have been achieved. It resulted in a best stabilized PCE of 21.03%, which is among the best for methylammonium-free PSC (see **Table S1**, Supporting Information). These PSCs are proved to be highly resistant to light, moisture, and temperature external stressors.

## 2. Experimental

The preparation of the fluorine-doped $SnO_2$ (FTO) substrates, de deposition of the 20 nm thick compact $TiO_2$ layer (*c*-$TiO_2$) by spray pyrolysis and the preparation of the 120 nm thick nanoparticle-based mesoporous $TiO_2$ layer by spin coating were performed as in our previous works.[7,29]

The basic protocol of $Cs_{0.1}FA_{0.9}PbI_3$ perovskite layer preparation was first to mix 156 mg of Formamidinium iodide (FAI, Greatcell), 461 mg of Lead iodide ($PbI_2$, TCI), 26 mg Cesium Iodide (CsI, TCI) in a 900 µL/100 µL of anhydrous DMF and DMSO solvent mixture. 45 µL of this solution was deposited on top of the substrate and the sample was first spun at 1000 rpm for 10 s and then at 4000 rpm for 20 s. The sample was treated by dripping 100 µL of anhydrous chlorobenzene 15s to 20s after the starting of the spinning routine. The film was finally annealed on a hotplate for 20 min at 155°C. For the AC film and KC film preparations, the procedure was the same except that 15 mg of $NH_4Cl$ and 6.7 mg of KCl, respectively, were added in the perovskite precursor solution. For the mixed-additive AKC film, the protocol was the same except that 15 mg of $NH_4Cl$ and 6.7 mg of KCl were added in the perovskite precursor solution. Full details on the PVK syntheses are provided in the **Section F** of the Supporting Information. The perovskite films thicknesses ranged between 360 nm and 400 nm in addition to the PVK filling the mesoporous $TiO_2$ layer.

*n*-propylammonium iodide (or propylamine hydroiodide, $CH_3CH_2CH_2NH_3I$), noted PAI, has been used in a few papers for the preparation of 2D/3D perovskite.[30, 31] It remains unexplored for the surface treatment of the perovskite layer since, to our knowledge, only Li et al. [19] report a PAI treatment to form an interfacial capping layer. In our work, 4 mg of PAI was dissolved in 1 mL isopropyl alcohol (IPA). 60 µL of this solution was deposited on the perovskite film after 2h-3h of cooling. The spin-coating program was run just after the solution deposition (2000 rpm/s acceleration, 3000 rpm for

20s). The 200 nm thick hole transporting material (HTM) layer was prepared as described in the Supporting Information.[32] The device was completed by a gold back contact with a thickness of 70-80 nm deposited by thermal evaporation.

The XRD patterns were measured by a PANanalytical X-Pert high-resolution X-ray diffractometer (XRD) operated at 40 kV and 45 mA and using the CuKα radiation with λ= 1.5406 Å. The morphology of perovskite thin films was observed using a field-emission SEM equipment (Zeiss Supra 40) in the in-lens mode. The EDX mapping spectra were measured with a Quantax system from Compact 30 mm Brucker operated at 15 kV. The differential scanning calorimetry (DSC) curves were measured on precipitated sample adducts by a DSC 3 apparatus from STAR System, operated under $N_2$ atmosphere with a heating rate of 10 °C $min^{-1}$. The solar cell was mounted on an O-ring at one side of the plasma chamber and was used as a cathode. The film specular absorbance was measured by a Cary 5000 UV-Vis-NIR spectrophotometer. A glass/FTO/*c*-$TiO_2$/*mp*-$TiO_2$ sample was employed for the baseline. The photoluminescence spectra were measured by a Cary Eclipse fluorescence spectrophotometer. The time-resolved photoluminescence (TRPL) curves were measured under a microscope (numerical aperture 0.7). The perovskites layers were spin-coated onto a glass/FTO/*c*-$TiO_2$/*mp*-$TiO_2$ substrate. The top of the PVK layers was excited by a 470 nm diode laser (Picoquant) and the emission was filtered by a 488-nm longpass filter. It was analyzed for time-resolved photoluminescence decay, by a PerkinElmer SPCM avalanche photodiode combined with a Picoharp acquisition card (500 ps characteristic time of the total system response function) used with the laser in a pulsed mode at a 10 nW excitation power (pulse duration 70 ps).

Up to now, GD-OES technique has been employed only in a few papers in connection with PSC half-cell [33] and full cells [25,34-36]. GD-OES experiments consisted in directly Ar-sputtering the devices to detect the optical emission of the elements etched-released from the various layers. It allowed to get the depth-profile distribution of the solar cell constituent elements. Moreover, by doing GD-OES profiling, before and after polarization, the profile change of iodide distribution due to migration has been disclosed.[25,35] Our GD-OES analyses were performed using a HORIBA Jobin Yvon GD Profiler 2 equipment. This instrument was equipped with a RF-generator (at 13.56 MHz), a standard HORIBA Jobin Yvon glow discharge source with a cylindrical anode of 4 mm internal diameter and two optical spectrometers (a polychromator and a monochromator) for fast-optical detection. The Ar plasma was generated at an Ar pressure of 420 Pa and an applied power of 17 W.

The solar cells *J-V* curves were recorded by a Keithley 2410 digital sourcemeter, using a 0.1 $V.s^{-1}$ voltage scan rate. The solar cells were illuminated with a solar simulator (Abet Technology Sun 2000) filtered to mimic AM 1.5G conditions (100 $mW.cm^{-2}$). The illuminated surface was delimited by a black mask with an aperture diameter of 3 mm. The power density was calibrated at 100 mW $cm^{-2}$ by the use of a reference silicon solar cell. For the statistical analysis, a minimum of 15 cells for each condition

were investigated and the results are provided in the Supporting Information. The EQE spectra were measured with an Oriel Instruments QuantX-300 system.

## 3. Results and Discussion

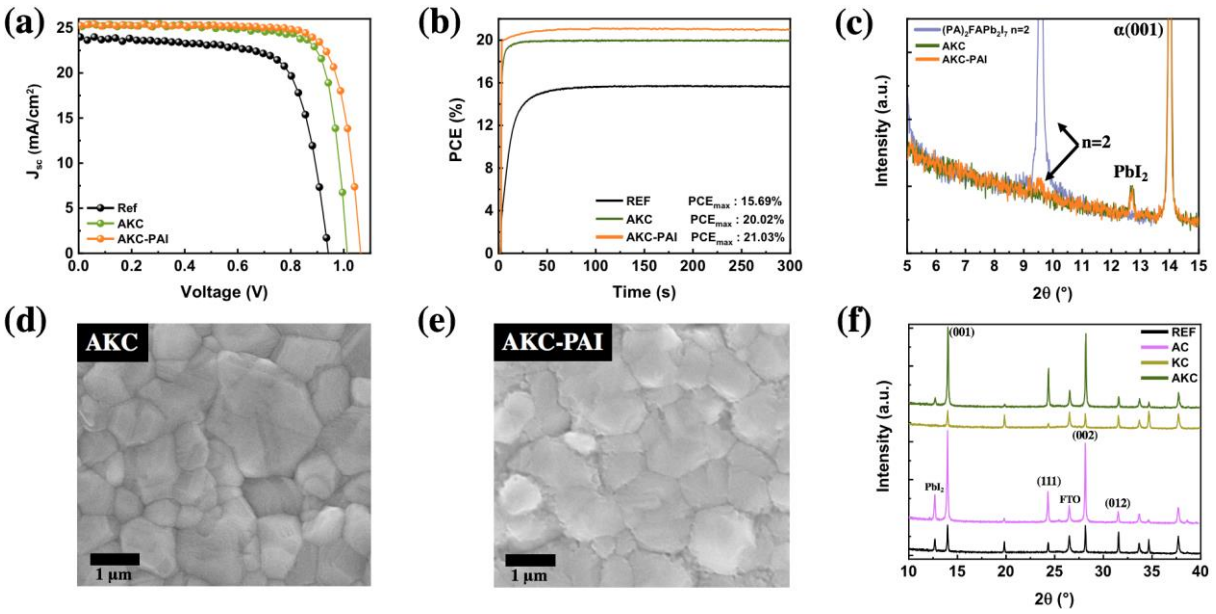


**Figure 1.** Effects of $Cs_{0.1}FA_{0.9}PbI_3$ engineering and capping layer on (a) the reverse scan *J-V* curves, (b) steady-state PCE at the maximum power point. (c) XRD patterns of the pristine and PAI treated AKC layer and of a 2D $(PA)_2FAPb_2I_7$ film. SEM layer top view before (d) and after (e) PAI treatment. (f) Effect of chloride additives on the XRD patterns.

**Table 1** summarizes the effect of employing chloride additives for the preparation of $Cs_{0.1}FA_{0.9}PbI_3$ perovskite films on the performances of solar cells with the configuration of compact $TiO_2$ (*c*-$TiO_2$)/mesoporous $TiO_2$ (*m*-$TiO_2$)/ perovskite/ 2,2',7,7'-tetrakis (N,N'-di-4-methoxyphenylamine)-9,9'-spirobifluorene (Spiro-OMeTAD)/Au as schematized in **Figure S1** (Supporting Information). The pristine cells (layers and cells hereinafter noted Ref) exhibited poor performances with a PCE at 16.2 % on the reverse scan (**Figure 1a**) and a large hysteresis. Using an optimized 30 mol% amount of $NH_4Cl$ additive in the PPS (see **Annex A** of the Supporting Information) resulted in a best PCE at 19.3% with a quite large hysteresis index (HI) of 18% (**Table 1**) (layers and cells hereinafter noted AC). KCl as a chloride additive was then investigated and the detailed study is reported in the **Annex B** of the Supporting Information. The best improvement was achieved for a KCl content at 9 mol % of molar $PbI_2$ content in the PPS (layers and cells hereinafter noted KC). The PCE achieved 19.1% with a very low HI at 1% (**Table 1**). The optimization of $NH_4Cl$/KCl additive mixtures is described in the **Annex C** (Supporting Information). An optimum for the open circuit voltage ($V_{oc}$), the short circuit current ($J_{sc}$) and the fill factor (*FF*) was found for $NH_4Cl$ at 30 mol% and KCl at 5 mol%. It resulted in a best PCE

measured on the reverse scan above 20% (**Table 1** and **Figure 1a**). Interestingly, this PCE was better than for the cells prepared with each individual chloride additive (**Table 1**) and both additives acted synergistically. This best composition has been retained in the rest of the paper and these PSCs and layer are noted AKC. The effect of additive on the devices performances was confirmed by the average values provided in **Table S3** (Supporting Information) and by measuring the stabilized efficiencies. We found 15.69 %, 18.71 %, 19.00 % and 20.02 % for Ref, AC, KC and AKC solar cells, respectively (**Figure 1b**).

**Table 1.** Champion $Cs_{0.1}FA_{0.9}PbI_3$ solar cells *J-V* curve parameters, PCE and hysteresis index.

| Name | Additive | Capping layer | Scan direction | $V_{oc}$ [V] | $J_{sc}$ [mA. cm$^{-2}$] | *FF* | PCE [%] | *HI(%)*[a)] |
|---|---|---|---|---|---|---|---|---|
| Ref | No | No | Reverse | 0.943 | 23.91 | 72.13 | 16.26 | 26 |
| | | | Forward | 0.846 | 23.83 | 59.36 | 11.96 | |
| AC | $NH_4Cl$ 30 mol% | No | Forward | 1.004 | 25.32 | 76.08 | 19.34 | 18 |
| | | | Reverse | 0.957 | 25.13 | 66.07 | 15.89 | |
| KC | KCl 9 mol% | No | Forward | 0.994 | 25.19 | 76.38 | 19.12 | 1 |
| | | | Reverse | 0.995 | 25.16 | 76.03 | 19.03 | |
| AKC | $NH_4Cl$ 30 mol% + KCl 5mol% | No | Forward | 1.014 | 25.23 | 78.69 | 20.13 | 4 |
| | | | Reverse | 1.012 | 24.96 | 76.84 | 19.41 | |
| AKC-PAI | $NH_4Cl$ 30 mol% + KCl 5mol% | Yes | Forward | 1.051 | 25.31 | 79.23 | 21.08 | 3 |
| | | | Reverse | 1.049 | 25.02 | 77.91 | 20.45 | |

[a)] Hysteresis Index, noted HI, defined as $(PCE_{Rev}-PCE_{For})*100/PCE_{Rev}$

To further improve the devices performances, the PVK surface was treated by a solution of *n*-propylammonium iodide (PAI) in isopropyl alcohol (IPA). The optimization and characterizations studies are detailed in the **Annex D** of the Supporting Information. The 4 mg.mL$^{-1}$ concentration resulted in the best PCE at 21.08% (**Table 1** and **Figure 1a**). The optimized treated films are noted AKC-PAI, hereafter. The beneficial effect of KCl additive was preserved since the hysteresis remained negligible with HI at 3% (**Table 1**). The significant improvement was confirmed by measuring the steady-state PCE (**Figure 1b**) which reached 21.03% for AKC-PAI, a value very close to the one measured on the *J-V* curve and gained 1% absolute compared to the untreated AKC cells. Combined scanning electron microscopy (SEM), x-ray diffraction (XRD) and absorbance analysis showed that this treatment generates a crystallized low-dimensional capping layer identified as $(PA)_2FAPb_2I_7$ by XRD (**Figure 1c-e** and **S11**, Supporting Information). The time-resolved photoluminescence (TRPL) curves of AKC and AKC-PAI samples are displayed in **Figure S13** (Supporting Information). They have been fitted by a

triple exponential function and the results are gathered in **Table S5** (Supporting Information). The fast time constant ($\tau_{fast}$) decreased from 1.9 ns to 1.2 ns with the PAI treatment. It shows a fast charge transfer toward the low-dimensional capping layer. The slow time constant ($\tau_{slow}$) is related with the perovskite film quality. It increased from 168 ns (Ref) to 551 (AKC) ns by using the mixed chloride additive. The PAI treatment resulted a further increase to 570 ns. This gain shows the passivation of defects in the perovskite film near the surface. We measured the $V_{oc}$ of Ref, AKC and AKC-PAI cells under various continuous light power densities ($I$). A white light source was employed, and the curves are disclosed in **Figure S14a** (Supporting Information). AKC cells exhibited higher $V_{oc}$ than the Ref one and the PAI-treated cell exhibited the highest $V_{oc}$ over all the investigated light intensity range. The $V_{OC}$ scaled logarithmically with $I$ and followed the relationship:

$$qV_{OC} = E_g + n_{ID}kT \ln(I/I_0) \quad (1)$$

with $q$ the elementary charge, $k$ the Boltzmann constant, $T$ the absolute temperature and $n_{ID}$ the ideality factor. $n_{ID}$ was determined from the curve fits. It is related to the main recombination phenomena occurring at the $V_{oc}$.[37-40] In classical semiconductor theory, a value of 1 for this parameter indicates a bimolecular recombination of free charges while a value of 2 reflects a monomolecular non-radiative recombination, typically a trap-assisted recombination through mid-gap states.[38,40] Deviation of $n_{ID}$ from 1 to 2 reflects the increasing occurrence of trap-assisted Shockley-Read-Hall (SRH) recombination through perovskite intragap defects.[37,38] $n_{ID}$ was measured at 1.98 for the Ref cell, 1.59 for the AKC cell and it decreased to 1.52 after the PAI treatment. It shows that interfacial recombinations are markedly depleted with the use of the mixed additive. The treatment is also beneficial because the presence of the $(PA)_2FAPb_2I_7$ layer favors the transfer to the HTM contact and then lowers recombinations. The beneficial effect of the PAI treatment has also been shown by measuring the dark current of AKC cells. In **Figure S14b** (Supporting Information) the PAI treatment reduces markedly the dark current and then recombinations occurring in the cells.

Our study highlights a major role of the chloride additives on the final performances of the PSCs which requires a detailed study focusing both on the final layers produced and on the effect of the additives on the film formation mechanism. Scanning electron microscopy (SEM) views of the reference layers showed small grains with mean size of 319 nm and the presence of pinholes (**Figure 2a**). The SEM cross-sectional views revealed multiple grain boundaries and the presence of voids at the perovskite/ $m$-$TiO_2$ interface (**Figure S15a,** Supporting Information). The XRD patterns disclosed peaks indexed by the perovskite α-phase (**Figure 1f**).[41] However, extra-peaks indexed by the $PbI_2$ parasitic phase were also present and the moderate peak intensity showed that the crystallinity of the sample was not very high. These features are detrimental for the performances. $PbI_2$ impurity phase was also detected on the XRD pattern in the AC sample (**Figure 1f and 2p)**. The most striking effect was that $NH_4Cl$ mediates the PVK crystals growth. It resulted in larger grain size with a mean value at 750 nm (**Figure**

**2b and 2e**). The films were texturised with the (00*l*) planes parallel to the substrate and they presented an improved crystallinity (**Figure 1f**). KCl additive provided a battery of beneficial effects: it prevented the formation of pinholes, of voids (**Figure 2c**) and of the formation of $PbI_2$ (**Figure 1f and 2o**). The layer was well-covering and was made of pure $Cs_{0.1}FA_{0.9}PbI_3$ photoactive α-phase. However, this additive did not improve the crystallinity and the PVK grains were still small with a mean size measured at about 387 nm (**Figure 2c and 2e**). Mixed additive film (AKC) retained the $NH_4Cl$ effect of mediating the formation of large grains with an average size of 935 nm (**Figure 2d and 2e**). The cross-sectional view (**Figure S15d**, Supporting Information) showed vertical grain boundaries and a monolithic structure, which is the desired one for high device efficiency. Moreover, AKC film XRD pattern exhibited a high crystallinity as found with $NH_4Cl$ additive (**Figure 1f and 2q**). The elemental composition of the various samples was mapped by energy-dispersive X-ray spectroscopy (EDX) (**Figure S16a-d**, Supporting Information). Pb, I and Cs were always detected. In contrast, Cl, present in a large amount as an additive in the AC, KC and AKC PPSs, was not detected in the final films either by EDX or GD-OES (**Figure S16**, Supporting Information). It means that chloride is almost fully eliminated upon the annealing step. On the other hand, the K element was present in the layers when KCl was used as an additive and it was distributed homogeneously in the prepared layers.[25]

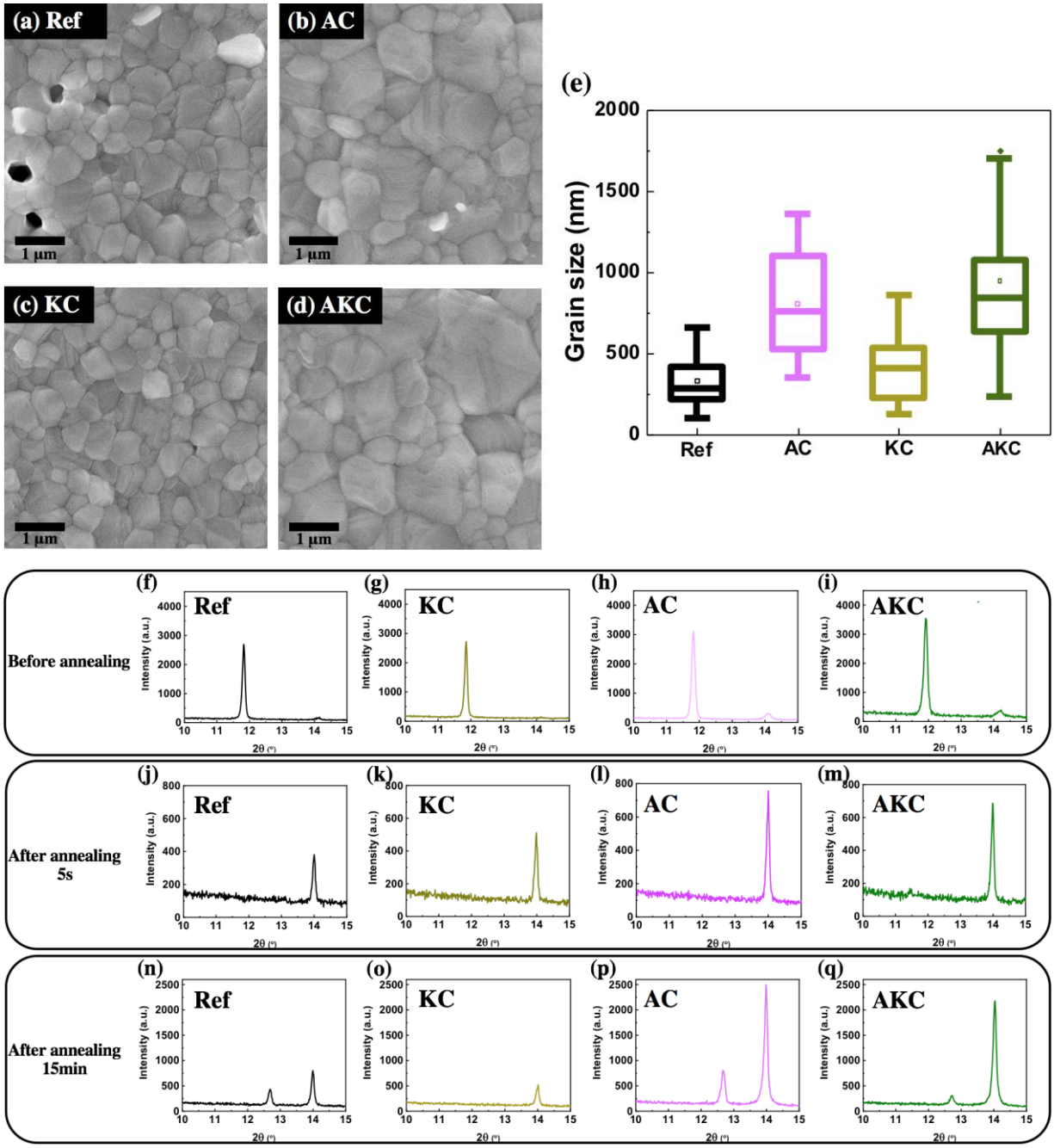


**Figure 2**. (a-d) SEM top-views of the $Cs_{0.1}FA_{0.9}PbI_3$ films. (e) Effect of chloride additives on the grain size. (f-m) Effect of chloride additives on the XRD pattern of the films produced by spin-coating, before annealing (f-i), after 5 s of annealing (j-m) and after (n-q) full annealing.

Ammonium and potassium chloride additives and their mixture control the perovskite film formation. To better understand the layer crystallization aspects, we compared the XRD patterns of the wet films obtained after spin-coating, after a 5 s annealing time and those resulting from a full thermal annealing treatment. The former patterns are displayed in **Figure 2f-i**. They all showed a main diffraction peak at 11.8° assigned to $Cs_{0.1}FA_{0.9}PbI_3$ δ-phase with hexagonal symmetry ((010) diffraction plane) ($P6_3mc$ space group).[41] This phase was more intense when $NH_4Cl$ was employed while KCl had no effect on

the initial phase. $NH_4Cl$ additive led also to the $Cs_{0.1}FA_{0.9}PbI_3$ α-phase initial presence as shown by the presence of a peak at about 14° assigned to its (001) reflection. XRD shows that the phase change to the photoactive α-phase occurred quickly, upon the first 5s of annealing at 155°C (**Figure 2j-m)**. We note that this peak was stronger when the α-phase was present originally. It then favored a higher film crystallinity.

Differential Scanning Calorimetry (DSC) was employed to further understand the effect of Cs, ammonium and chloride ions on the formation of the crystallized perovskite. The curves were measured on the four samples prepared as powders adducts (**Figure 3a-d)**, completed by a $FAPbI_3$ powder adduct for reference (**Figure S17,** Supporting Information). A first endothermic peak was observed at ~70°C-90°C, assigned to the evaporation of DMSO (DMF was eliminated upon washing the adducts by diethyl ether)[42] since DMSO mixed with $PbI_2$ has been shown to start to evaporate at a temperature as low as 75°C.[43] First, a higher peak temperature was found for $FAPbI_3$ (82.7°C) compared to $Cs_{0.1}FA_{0.9}PbI_3$ (78.5°C). It suggests that the presence of CsI weaken the DMSO bonding. The evaporation temperature did not change significantly with the chloride additives ($NH_4Cl$, KCl or both). For $FAPbI_3$ sample, an endothermic peak was observed at 101.5 °C which is attributed in the literature to the crystallization of the perovskite yellow δ-phase.[43,44]. In the case of $Cs_{0.1}FA_{0.9}PbI_3$ samples, this peak was not visible. Above 100°C, an extended endothermic feature was found, assigned to the crystallization/phase change to the α-phase perovskite compounds from the precursor. In the case of $FAPbI_3$, it extended up to 162°C with a minimum at 153.5°C. This minimum can be roughly taken as the temperature at which the crystallization and growth steps end and allows a clear comparison between the samples. Adding CsI significantly reduced this temperature at 137.3 °C. Also, a low temperature was found for KCl additive (minimum at 132.4°C). Therefore, in both cases (Ref and KC), a fast crystallization and growth occured. On the other hand, $NH_4Cl$ additive delays and slows down the perovskite crystal growth and it favors the formation of large grains. This effect of $NH_4Cl$ was also observed by *in-situ* microscopy in the case of $MAPbI_3$ perovskite by Dai et al..[45]

The residual solvent elimination is an important occurrence upon the film crystallization and growth. To our knowledge, the present work is the first to use the GD-OES technique to follow the depth profile of the solvent leaving by evaporation upon the annealing of a perovskite film. Indeed, the solvent employed is a DMF-DMSO mixture and S element contained in DMSO can be tracked by this technique. The S element profile for the various films and various annealing times are presented in **Figure 3e-l**. By increasing the sputtering time, deeper part of the PVK layer is analyzed until reaching the *meso*-$TiO_2$ layer (dashed black line in **Figures 3e-h**). Before annealing, the DMSO profile is asymmetrical in every case, and we observe that the outer part of the film is richer in solvent than the inner part. For the annealing, our results distinguish two stages. The first one occurs during the first 5 seconds of annealing on a hotplate. The initial film changes from yellow translucent to brown. During this stage, the most superficial residual solvent evaporates and is almost fully eliminated at the uttermost surface while the

$Cs_{0.1}FA_{0.9}PbI_3$ present in the wet layer is fully transformed into the α-phase (**Figure 2j-m**). The Ref sample is the only one for which the inner solvent is not partially eliminated but entrapped during this step. The next stage corresponds to 5s to 30s annealing times, when the film becomes dark-brown. We observed a clear effect of the additive on the solvent distribution upon annealing. In the case of the Ref sample, DMSO is eliminated fast near the surface while it remains in the deeper part of the layer. The same behavior is observed for the KC sample. For these two films, the grains grow downward, from the top to the bottom. It favors the multiple and oblique grain boundaries and rather small perovskite grains are produced. In the presence of AC, the profiles are different. For AC, the S profile is more extended throughout the layer thickness. For the double additives (AKC), the solvent profile decreases uniformly throughout the layer thickness. In this case a bulk grain lateral growth occurs, and it results in more homogeneous films with big monolithic grains as shown by SEM (**Figure S15**, Supporting Information). In all cases, the solvent was fully eliminated after 2 min (**Figure S18**, Supporting Information). A striking result of this study is that the additive mixture regulates the homogeneous solvent elimination and then the growth of the film in its full depth. It boosts the quality of the film.

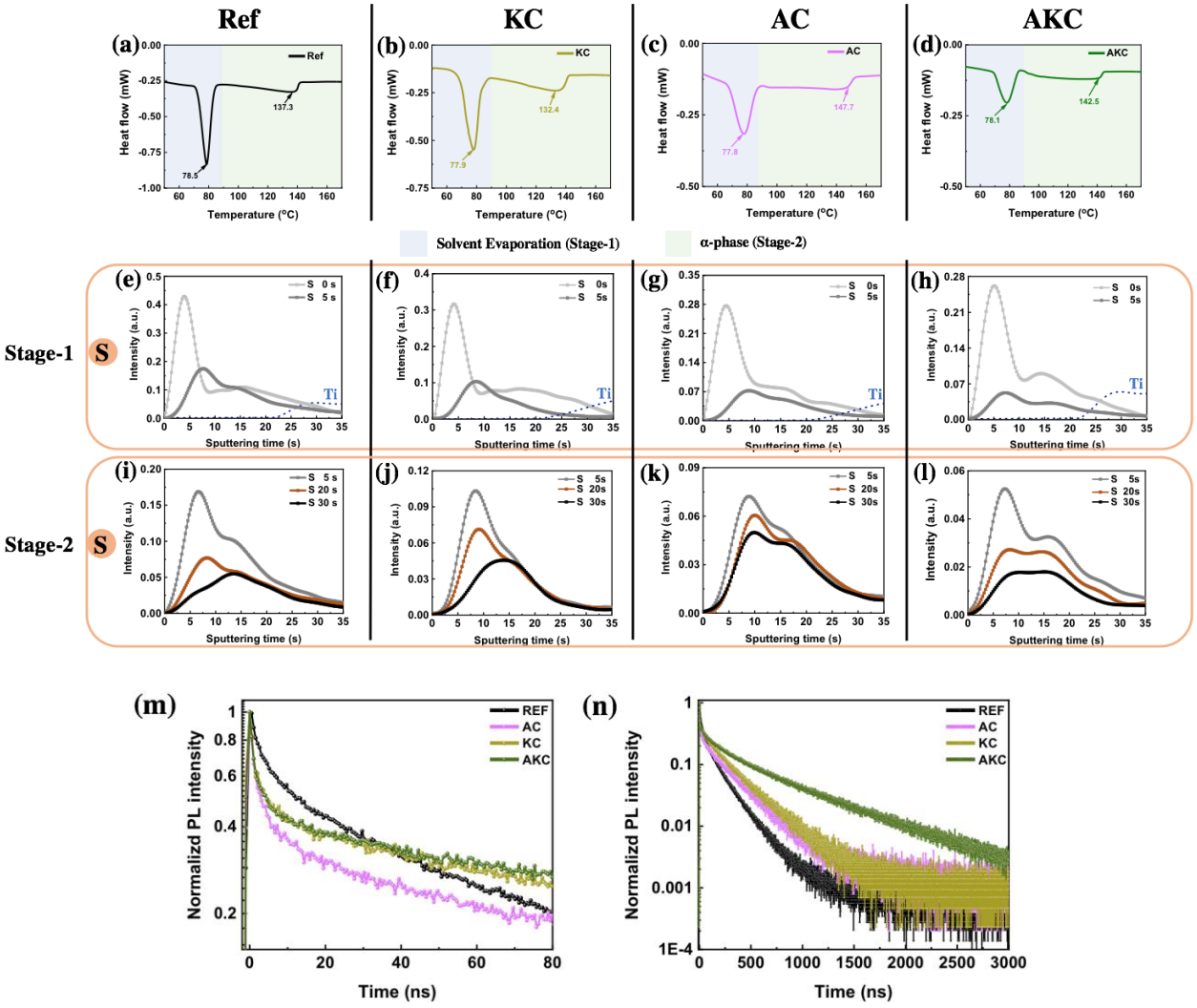

**Figure 3.** (a-d) DSC curves of $Cs_{0.1}FA_{0.9}PbI_3$ adducts prepared with various additives. (e-l) Evolution of GD-OES sulphur element (S) profile in the perovskite precursor layer upon annealing. (Dashed line in (e-h): Ti profile corresponding to the *meso*-$TiO_2$). (m,n) Effect of additives on the TRPL curves of PVK layers.

When the growth is regulated by the co-additive, the monolithic structure, which is the targeted one for high performances, is achieved. Voids and pinholes are eliminated, the films are more homogeneous, and the density of defects is reduced. The latter is shown by further scrutinizing TRPL measurements **(Figure 3m,n** and **Annex E**, Supporting Information). $\tau_{slow}$ was measured at 168 ns for the reference sample and at 243 ns and 254 ns for the AC and KC films, respectively. By mixing both potassium and ammonium chloride, we achieved a remarkable 551 ns value. It demonstrates that very high bulk perovskite quality was achieved then. It is conspicuous that additives reduce the structural defects in the methylammonium-free perovskite.

This study illustrates that grain growth is linked to the solvent elimination from the film and we can distinguish different cases as schematized in **Figure 4**. For the Ref sample, the solvent evaporation mainly occurs at the film surface. Film grows downward, multiple-boundaries perovskite grains are formed while the solvent in the inner part of the film remains entrapped and is at the origin of void formation and poor *m*-$TiO_2$/perovskite interface. In the case of the KC sample, the solvent is better eliminated but the film still grows downward, and the it is formed of multiple-boundaries grains. For double ammonium chloride and potassium chloride additives (AKC samples), the solvent is homogeneously eliminated in the depth of the film which leads to the lateral growth of the grains and results in monolithic large grains with low defect density. It is the targeted morphology for high efficiency. Finally, the AC film formation mechanism is intermediate between KC and AKC.

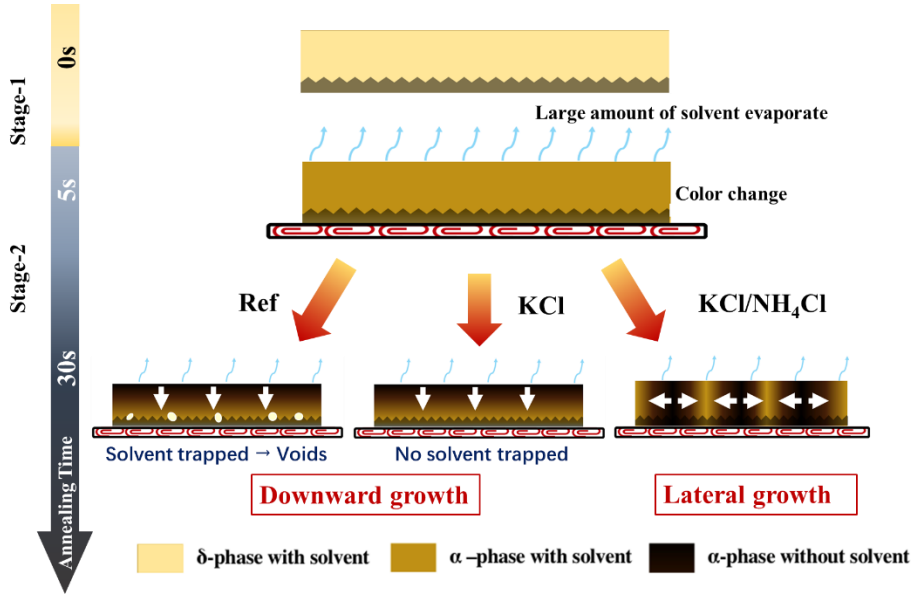

Cite this paper as : D. Zheng, T. Pauporté, Control by Mixed-Chloride Additives of the Quality and Homogeneity of Bulk Halide Perovskite upon Film Formation Process. J. Mater Chem. A 9 (2021) 17801-17811.

**Figure 4**. Schematic of the film formation processes observed without additive (Ref), with KCl additive and with mixed-chloride additives: Grain growth direction and mechanism.

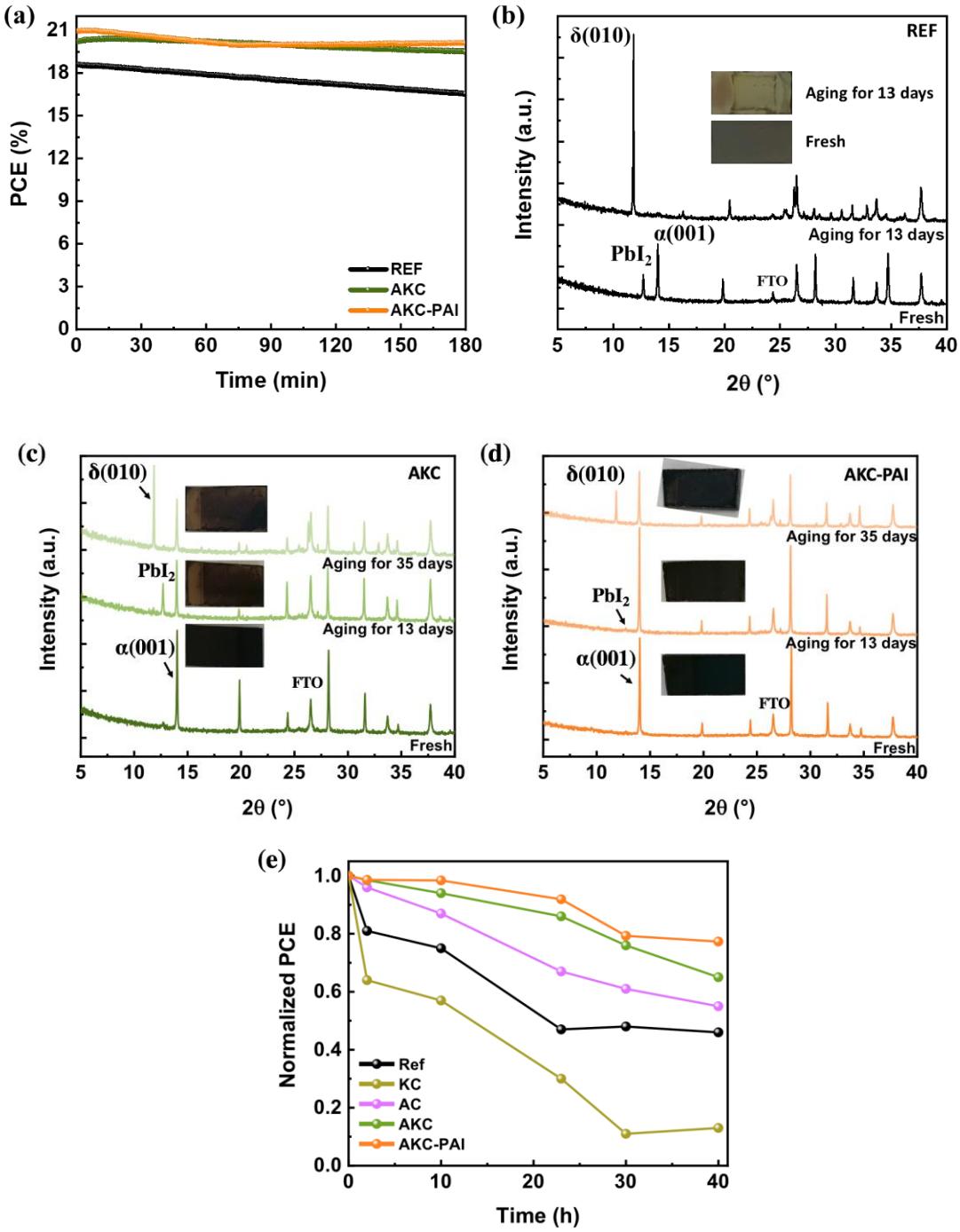


**Figure 5:** (a) Tracking of the Ref, AKC and AKC-PAI cells at their maximum power point; (b-d) XRD patterns of the (b) Ref, (c) AKC and (d) AKC-PAI layers under ambient condition (20°C, 55±10% RH). The insets are layers pictures. (e) Normalized PCE evolution of cells stored under ambient condition and very high humidity (RH≥90%).

The future of the PSC technology will depend on the ability of scientists to develop devices highly resistant to heat, moisture, and light and which stand long-term operation. This led us to evaluate the effect of our double engineering approach on the stability toward various degradation agents. First, the stability of unencapsulated cells under one sun illumination was followed by tracking at their maximum power point (MPP). **Figure 5a** shows that the Ref cell was poorly stable since its PCE continuously decreased upon the test. The stability was markedly increased by using the double chloride additives. Finally, the PAI-treated cell was the most efficient and stable. After a small PCE decrease during the first 70 min, the PCE increased slowly for the next hours. It suggests some initial interfacial reorganization before stabilization and improvement. If we compare with other perovskites published by the group [46] (**Figure S19**, Supporting Information), only the $FA_{0.94}MA_{0.06}PbI_3$ cell exhibited such high stability while the PCE of the $MAPbI_3$ and $Cs_{0.08}FA_{0.80}MA_{0.12}Pb(I_{0.88}Br_{0.12})_3$ cells continuously decreased.

We also implemented accelerated aging tests. The thermal stability was investigated by heating the layers at 130°C for 4h in a $N_2$-filled glovebox. The results, disclosed in **Figure S20** (Supporting Information), show that $PbI_2$ is the heating degradation product of α-$Cs_{0.1}FA_{0.9}PbI_3$. The Ref sample was the less stable with a large increase of the $PbI_2$ diffraction peaks. Using the chloride mixed-additives led to films with less initial $PbI_2$, to a decrease of the $PbI_2$ formation by heating and then slowed down the thermal degradation. The capping layer further suppressed the degradation and the AKC-PAI layer was much more stable than the Ref one. After 4 hours, the PVK/$PbI_2$ peak ratio (at 13.9° and 12.7°) was 3.4 for AKC sample and 4.6 for the AKC-PAI sample. The aging of the layers stored under ambient air (20°C, 55±10% relative humidity (RH)) was followed by XRD. **Figure 5b-d** shows that the Ref sample was fully degraded after only 13 days. The degradation product was the δ-phase in this case which is the phase stable at room temperature. The employment of the chloride additives was of great effectiveness since the α-phase was still present after 35 days in the AKC sample even if the δ-phase (010) peak was more intense then than the α-phase (001) one. The interesting point is that the capping layer further increased the stability. After 13 days of aging, the XRD pattern was unchanged. After 35 days, the sample was still black colored and the most intense diffraction peaks were those of the α-phase.

Getting PSCs highly stable under high moisture is the trickiest issue because PVKs form hydrate compounds in the presence of humidity.[47,48] We performed a highly demanding test by following unencapsulated cells aged under high humidity environment (RH≥90%, the other conditions being ambient) for several days. **Figure 5e** presents the normalized PCE of Ref, KC, AC, AKC and AKC-PAI cells. A first very interesting observation is that the KC cell was the less stable. On the other hand, getting large grains with $NH_4Cl$ additive was beneficial for the stability against humidity. The stability was better when the two chloride additives were mixed. The remarkable result is that coupling the mixed chloride additives and the surface treatment even further improved the stability of the cells. The unencapsulated AKC-PAI cells retained about 80% of their initial PCE after 40 h of aging in this case.

This stability result is much better than those we obtained for optimized MA-containing perovskites, namely $MAPbI_3$, $Cs_{0.08}FA_{0.80}MA_{0.12}Pb(I_{0.88}Br_{0.12})_3$ and $FA_{0.94}MA_{0.06}PbI_3$, published in Ref.[46] and presented in **Figure S21** (Supporting Information). The best of them retained less than 60 % of its initial PCE after 40 h of aging. This test, performed under highly demanding conditions, is an accelerated one, and one can expect a much better stability for devices after their *ad hoc* encapsulation.

## 3. Conclusions

In summary we have developed a two-steps engineering approach for the preparation of MA-free and Br-free $Cs_{0.1}FA_{0.9}PbI_3$ perovskite films for PSC application. Introducing the mixed $NH_4Cl$ and KCl additives in the PPS to assist the PVK formation allowed us to get films with outstanding properties. The former, employed at large mol %, led to a good film coverage, large grains, good crystallinity and reduced structural defects. The second also reduced the structural defects, reduced the $PbI_2$ phase content and suppressed the hysteresis. By combining XRD, SEM, DSC and GD-OES techniques the effects of the additives on the film formation mechanism and grain growth direction have been unveiled. The initial yellow translucent layer formed by spin-coating contains $Cs_{0.1}FA_{0.9}PbI_3$ in the δ-phase and in the α-phase combined with wetting residual solvent. During the first 5s of annealing time, the δ-phase is transformed into the α-phase and the surface solvent is greatly eliminated. Then the profile of the solvent elimination has allowed us to understand the final properties of the layers. When the solvent in the deep is difficult to eliminate, the growth occurs downward, voids at the perovskite/oxide, small grains and oblique multiple-grain boundaries are formed. When the elimination speed decreases with the depth without entrapped solvent, the same morphology is obtained without voids. Finally, using both $NH_4Cl$ and KCl (and in a less extend only $NH_4Cl$) allows to uniformly eliminate the solvent and then achieve a lateral growth of the perovskite grains. It results in vertical grain boundaries along with large, monolithic and defect-poor grains with good coverage of the substrate. Combining the later type of growth with the film surface treatment with *n*-propylammonium iodide (PAI), resulted in a record stabilized PCE of 21.03%. Finally, we have proved that the optimized films are highly resistant to electrical, light, moisture, and temperature external stressors and that this resistance is reinforced by the capping interfacial layer.

## ASSOCIATED CONTENT

**Supporting Information** to this paper can be found online. Review of high efficiency MA-free PSCs; Schematic diagram of the perovskite solar cell structure; Effect of $NH_4Cl$ additive on SEM view and grain size of PVK layers; Effect of $NH_4Cl$ additive on XRD patterns, absorbance and photoluminescence spectra of $Cs_{0.1}FA_{0.9}PbI_3$ layers; Statistical analysis of the effect of $NH_4Cl$ additive on the *J-V* curve

parameters; Effect of KCl on SEM top view images of $Cs_{0.1}FA_{0.9}PbI_3$ layers and XRD patterns; Effect of potassium chloride additive on the absorbance and steady-state photoluminescence spectra of PVK layers; Statistical analysis of the effect of KC additive on the *J-V* curve parameters; Statistical analysis of the effect of KC and $NH_4Cl$ additive mixtures on the *J-V* curve parameters Table of best *J-V* curve parameters of mixed additive; Table of J-V parameters of champion and average PSCs; Effect of PAI concentration in IPA on the *J-V* curves parameters of AKC-PAI cells; Statistical analysis of the *J-V* curve parameters and EQE of AKC-PAI and AKC cells; Effect of AKC film post-treatment on XRD, photoluminescence, absorbance and differential absorbance of the films; Effects of additives on absorbance and Tauc plots; Triple-exponential function fitting parameters of the TRPL decay curves;; Effect of surface treatment on TRPL curves; *Voc* versus light intensity of PSCs; Dark J-V curves; Effect of additives on film SEM cross-sectional views; EDX elements mapping results of the perovskite layers; GD-OES curve of Cl element (AKC sample); DSC curve of $FAPbI_3$ adduct; Effect of additive on the GD-OES curves up to 2 min; Tracking under 1 sun of optimized MA-containing PSCs; Effect of layer heating at 130°C for 4h on the XRD pattern; Evolution of J-V curve parameters of MA-containing cells exposed to 90 % RH; Complementary experimental.

## AUTHOR INFORMATION

### Corresponding Author

* thierry.pauporte@chimieparistech.psl.eu

### Authors Contributions

Daming Zheng: Conceptualization, Investigation, Data analysis, Writing; Thierry Pauporté: Supervision, Data analysis, Writing, Reviewing and Editing.

### Notes

The authors declare no competing interests.

## ACKNOWLEDGMENTS

Dr. Philippe Vermaut (IRCP, Chimie-paristech, France) is acknowledged for access to the DSC 3 apparatus from STAR System. Mr J. Liu (Institut des NanoSciences de Paris, Sorbonne Université, France) is acknowledged for some TRPL measurements. The Ph.D scholarships of Mr D. Zheng was

funded by the CSC-Paristech program (grant number 201806310126). The ANR agency is acknowledged for financial support via the Moreless project ANR-18-CE05-0026.

**References**

[1] M. M. Lee, T. Miyasaka, T. N. Murakami, *Science*, 2012, **338**, 643-647.
[2] H. S. Kim, C. R. Lee, J. H. Im, K. B. Lee, T. Moehl, A. Marchioro, S. J. Moon, R. Humphry-Baker, J. H. Yum, J. E. Moser, M. Gratzel, N. G. Park, *Sci. Rep.*, 2012, **2**, 591.
[3] J. Burschka, N. Pellet, S. J. Moon, R. Humphry-Baker, P. Gao, M. K. Nazeeruddin, M. Gratzel, *Nature*, 2013, **499**, 316.
[4] H. P. Zhou, Q. Chen, G. Li, S. Luo, T. B. Song, H. S. Duan, Z. R Hong, J. B. You, Y. S. Liu, Y. Yang, *Science*, 2014, **345**, 542.
[5] J. Zhang, P. Barboux, T. Pauporté, *Adv. Energy Mater.*, 2014, **4** , 1400932.
[6] J. Zhang, E. J. Juárez-Pérez, I. Mora-Seró, B. Viana, Th. Pauporté, *J. Mater. Chem.* A, 2015, **3**, 4909–4915.
[7] P. Wang, Z. Shao, M. Ulfa, T. Pauporté, *J. Phys. Chem. C*, 2017, **121**, 9131–9141.
[8] T. Zhu, J. Su, F. Labat, I. Ciofini, Th. Pauporté, *ACS Appl. Mater Interfaces*, 2020, **12**, 744-752.
[9] F. Zhang, K. Zhu, *Adv. Energy Mater.*, 2020, ***10***, 1902579.
[10] NREL Chart (January 2021) https://www.nrel.gov/pv/cell-efficiency.html
[11] M. Abdelsamie, J. Xu, K. Bruening, C. J. Tassone, H. G. Steinrück, M. F. Toney, *Adv. Funct. Mater.*, 2020, 2001752
[12] S. Chen, X. Xiao, B. Chen, L. L. Kelly, J. Zhao, Y. Lin, M. F. Toney, J. Huang, *Sci. Adv.*, 2021, **7**, eabb2412.
[13] D. Y. Son, S. G. Kim, J. Y. Seo, S. H. Lee, H. Shin, D. Lee, , N. G. Park *J. Am. Chem. Soc.*, 2018, **140**, 1358.
[14] L. L. Gao, I. Spanopoulos, W. J. Ke, S. Huang, I. Hadar, L. Chen, X. L. Li, G. J. Yang, M. G. Kanatzidis, *ACS Energy Lett.*, 2019, **4**, 1763.
[15] P. Chen, Y. Bai, S. C. Wang, M. Q. Lyu, J. H. Yun, L. Z. Wang, *Adv. Funct. Mater.*, 2018, *28*, 1706923
[16] W. M. Ming, S. Y. Chen, M. H. Du, *J. Mater. Chem. A*, 2016, **4**, 16975-16981.
[17] S. H. Turren-Cruz, A. Hagfeldt, M. Saliba, *Science*, 2018, **362**, 449-453.
[18] Y. H. Park, I. Jeong, S. Bae, H. J. Son, P. Lee, J. Lee, C. H. Lee, M. J. Ko, *Adv. Funct. Mater.*, 2017, **27**, 1605988.
[19] S. D. Li, Z. Liu, Z. Qiao, X. Wang, L. Cheng, Y. F. Zhai, Q. F. Xu, Z. M. Li, K. Meng, G. Chen, *Adv. Funct. Mater.*, 2020, 2005846.
[20] J. C. Germino, R. Szostak, S. G. Motti, R. F. Moral, P. E. Marchezi, H. S. Seleghini, L. G. Bonato, F. L. de Araujo, T. D. Z. Atvars, L. M. Herz, D. Fenning, Hagfeldt, A. F. Nogueira, *ACS Photonics*, 2020, **7**, 2282-2291.
[21] P. C. S. Schulze, A. J. Bett, M. Bivour, P. Caprioglio, F. M. Gerspacher, O. Kabaklı, A.; R. Q. Zhang, M. Hermle, H. Hillebrecht, Stefan, S. W. Glunz, J. C. Goldschmidt, *Sol. RRL*, 2020, **4**, 2000152
[22] S. Kelly, K. Pabitra, Nayak, Alexandra, J. Ramadan, B. Wenger, Y. Lin, H. Snaith, *Adv. Funct. Mater.*, 2019, **29**, 1900466
[23] J. Yang, Y. Chen, W. Tang, S. Wang, Q. Ma, Y. Wu, N. Yuan, J. Ding, W. H. Zhang, *J. Energy Chem.*, 2020, **48**, 217-225.
[24] S. Zhang, S. Wu, R. Chen, W. Chen, Y. Huang, Z. Yang, W. Chen, *J. Mater. Chem. C*, 2020, **8**, 1642-1648.
[25] D. Zheng, T. Zhu, T. Pauporté, *Solar RRL*., 2021, **5**, 2100010.

[26] Z. Li, N. Liu, Z. Liu, X. Wang, Y. Hu, Q. F. Xu, S. D. Li, Z. Qiao, L. Cheng, C. W. Wang, K. Meng, G. Chen, *Energy Tech.*, 2020, **8**, 2000224.
[27] X. Zhao, C. Yao, K. Gu, T. Liu, Y. Xia, Y. L. Loo, *Energy Environ. Sci.*, 2020, **13**, 4334-4343.
[28] N. Li, Y. Luo, Z. Chen, X. Niu, X. Zhang, J. Lu, Kumar, R. J. Jiang, H. Liu, X. Guo, B. Lai, G. Brocks, Q. Chen, S. Tao, D. P. Fenning, H. Zhou, *Joule*, 2020, **4**, 1743-1758.
[29] P. Wang, M. Ulfa and T. Pauporté, *J. Phys. Chem. C* 2018, *122*, 1973−1981.
[30] D. Yao, C. Zhang, S. Zhang, Y Yang, A. Du, E. Waclawik, X. Yu, G. J. Wilson, H. Wang, ACS *Appl. Mater. Interfaces* 2019, **11**, 29753−29764.
[31] C. Fei, M. Zhou, J. Ogle, D.-M. Smilgies, L. Whittaker-Brooks, H. Wang, *J. Mater. Chem. A*, 2019, **7**, 23739-23746.

[32] T. Zhu, D. Zheng, M.-N. Rager, Th. Pauporté, *Sol. RRL*, 2020, **4**, 2000348.
[33] L. Cojocaru, S. Uchida, D. Matsubara, H. Matsumoto, K. Ito, Y. Otsu, P. Chapon, J. Nakazaki, T. Kubo, H. Segawa, *Chem. Lett*. 2016, **45**, 884–886.
[34] Z. Ahmad, M. A. Najeeb, R. A. Shakoor, A. Alashraf, Al-Muhtaseb, S. A. Ahmed Soliman, M. K. Nazeeruddin, *Sci. Rep*. 2017, **7**, 15406.
[35] H. Lee, S. Gaiaschi, P. Chapon, A. Marronnier, H. Lee, J. C. Vanel, D. Tondelier, J.-E. Bourée, Y. Bonnassieux, B. Geffroy, *ACS Energy Lett*. 2017, **2**, 943−949.
[36] H. Lee, S. Gaiaschi, P. Chapon, D. Tondelier, J.-E. Bourée, Y. Bonnassieux, V. Derycke, B. Geffroy, *J. Phys. Chem. C* 2019, **123**, 17728−17734.
[37] W. Tress, M. Yvari, K. Domanski, P. Yadav, B. Niesen, J.P. Correa Baena, A. Hagffeldt, M. Graetzel, *Energy Environ. Sci*. 2018, **11**, 151–165.
[38] P. Caprioglio, C. M. Wolff, O.J. Sandberg, A. Armin, B. Rech, S. Albrecht, D. Neher, M. Stolterfoht, *Adv. Energy Mater*. 2020, **10**, 2000502.
[39] P. Calado, D. Burkitt, J. Yao, J. Troughton, T. M. Watson, M. J. Carnie, A. M. Telford, B. C. O'Regan, J. Nelson, P.R.F. Barnes, *Phys. Rev. Appl*. 2019, **11**, 044005.
[40] Contreras-Bernal, L.; Salado, M.; Todinova, A. ; Calio, L. ; Ahmad, S.; Idigoras, J.; Anta, J.A. J. Phys. Chem. C 2017, 121, 9705-9713.
[41] Q. Han, S. Bae, P. Sun, Y. Hsieh, Y. Yang, Y. Rim, H. Zhao, Q. Chen, W. Shi, G. Li, Y. Yang, *Adv. Mater.*, 2016, **28**, 2253–2258
[42] G. Grancini, Roldán-Carmona, C. I. Zimmermann, E. Mosconi, X. Lee, D. Martineau, S. Narbey, F. Oswald, F. De Angelis, M. Graetzel, M. K. Nazeeruddin, *Nature Commun.*, 2017, **8**, 15684;
[43] W. S. Yang, J. H. Noh, N. J. Jeon, Y. C. Kim, J. Ryu, S. Seo, S. I. Seok, *Science*, 2015, **348**, 1234.
[44] J. W. Lee, D. J. Seol, A. N. Cho, N. G. Park, *Adv. Mater.*, 2014, **26**, 4991-4998.
[45] X. Dai, Y. Deng, C. H. Van Brackle, S. Chen, N. Peter, X. Rudd, Y. Xiao, B. Chen, J. Huang, *Adv. Energy Mater.*, 2020, **10**, 1903108.
[46] D. Zheng, T. Zhu, T. Pauporté, *ACS Appl. Energy Mater*. 2020, **3**, 10349−10361
[46] D. Zheng, C. Tong, T. Zhu, Y. Rong, Th. Pauporté, *Nanomaterials*, 2020, **10**, 2512.
[47] A. Leguy, Y. Hu, M. Campoy-Quiles, M. I. Alonso, O. J. Weber, P. Azarhoosh, M. van Schilfgaarde, M. T. Weller, T. Bein, J., Nelson,Pablo Docampo, R.F. Piers Barnes, *Chem. Mater.*, 2015, **27**, 3397–3407.

Cite this paper as : D. Zheng, T. Pauporté, Control by Mixed-Chloride Additives of the Quality and Homogeneity of Bulk Halide Perovskite upon Film Formation Process. J. Mater Chem. A 9 (2021) 17801-17811.

**TOC Entry**

The roles of mixed ammonium chloride and potassium chloride additives on the growth of $Cs_{0.1}FA_{0.9}PbI_3$ perovskite film is investigated along with the surface treatment by a n-propylammonium iodide solution which produces an interfacial buffer layer. The optimized perovskite solar cell reaches a stabilized power conversion efficiency over 21%.